

Electronic Supplementary Information:
Resistive pressure sensors based on freestanding
membranes of gold nanoparticles

Hendrik Schlicke, Matthias Rebber, Svenja Kunze, and Tobias Vossmeier*

*Institute of Physical Chemistry, University of Hamburg, Grindelallee 117, 20146 Hamburg,
Germany*

E-mail: tobias.vossmeier@chemie.uni-hamburg.de

*To whom correspondence should be addressed

Gold nanoparticles

Dodecylamine stabilized gold nanoparticles (GNPs) were used for membrane fabrication. The GNPs were prepared following a synthetic route published by Leff et al.¹ Transmission electron microscopy was conducted for determining the GNP sizes, using a Philips CM 300 microscope, operated at 200 kV. In order to improve the stability of the particles prior to TEM characterization, the dodecylamine ligands were exchanged by dodecanethiol, as we described previously.² Figure S1 shows a representative transmission electron micrograph and a size histogram. An average particle diameter of (3.5 ± 0.7) nm was found. Particles with diameters < 1 nm were excluded from sizing statistics.

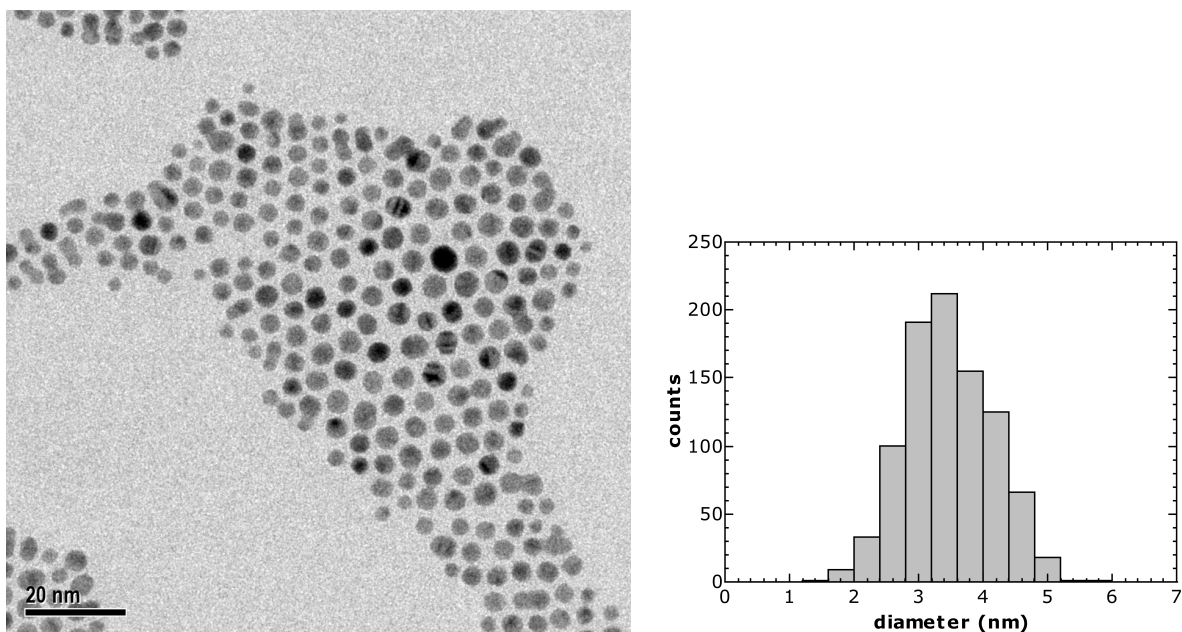


Figure S1: Transmission electron micrograph (*left*) and size histogram (*right*) of the GNP batch used for GNP membrane fabrication in this study.

UV/Vis spectroscopy of cross-linked GNP-films

A UV/Vis absorbance spectrum of the as-deposited 1,6-hexanedithiol (6DT) cross-linked GNP film on a glass substrate is depicted in Figure S2. Compared to the solution phase spectrum of the GNPs (dashed gray line), the plasmon band is red shifted due to the short interparticle distances resulting in plasmonic interactions.

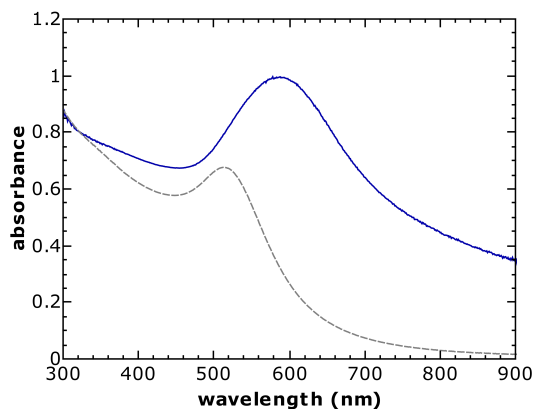


Figure S2: UV/Vis absorbance spectrum of the GNP membrane used for fabrication of the pressure sensor. A solution-phase spectrum of the GNPs is shown as dashed gray line (dilution $f = 1/600$).

Film thickness measurements (AFM)

For thickness measurements, sections of the as-deposited GNP film on a glass substrate were scratched using a cannula. Three AFM scans were conducted at different locations at the film edges using a DI Multimode AFM equipped with a Nanoscope IV controller and a 100 μm scanner. From each scan, five step-profiles were obtained and step-height values were extracted and averaged. Figure S3 shows the AFM scans recorded for film thickness measurement. An average thickness of $t = (55 \pm 1)$ nm was measured.

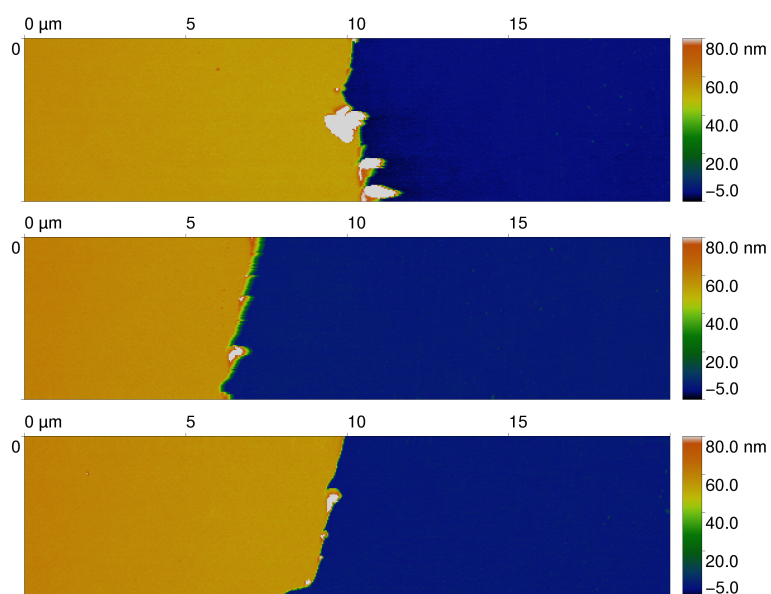


Figure S3: AFM scans ($20 \times 5 \mu\text{m}^2$) of GNP film sections used for thickness measurements.

Charge transport measurements

A section of the as-prepared substrate-supported GNP-film was investigated regarding its charge transport properties. Gold electrodes (~ 100 nm thickness) were deposited onto the film section by thermal evaporation, using a cannula (outer diameter $0.4\ \mu\text{m}$) as a shadow mask. Current-voltage (IV) data were measured by using an Agilent 4156C semiconductor parameter analyzer. The sample clearly showed ohmic behavior, see figure S4.

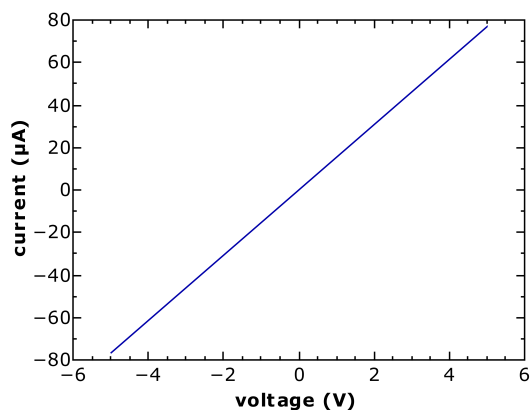


Figure S4: Current-voltage characteristics of the 55 nm thick GNP film used for fabrication of the pressure sensor (electrode geometry: $411\ \mu\text{m}$ channel length, $0.9\ \text{cm}$ channel width), corresponding to a conductivity of $0.1\ \text{S cm}^{-1}$.

Investigation of mechanical properties

For the model describing the sensor response, a biaxial modulus of 8.9 GPa for 6DT interlinked GNP membranes was used as an input parameter. This value was determined by bulge testing of 6DT interlinked GNP membranes as described in an earlier study for 1,9-nonanedithiol (9DT) interlinked GNP membranes.³

For bulge testing, sections of 6DT interlinked GNP films were transferred to substrates, having circular apertures with a diameter of $\sim 100 \mu\text{m}$. The membranes were then bulged by applying a varying nitrogen overpressure to their backside and the resulting membrane bulges were monitored using tapping mode atomic force microscopy (AFM, JPK Nanowizard). By analyzing the pressure-dependent topography data applying the “circular fit method”, stress-strain diagrams (as exemplarily shown in figure S5) were extracted. Slope fits of the stress-strain data collected from 4 membranes yielded an average biaxial modulus of (8.9 ± 0.6) GPa.⁴ A more detailed description of the bulge test procedure and data evaluation method is provided in our previous publication.³

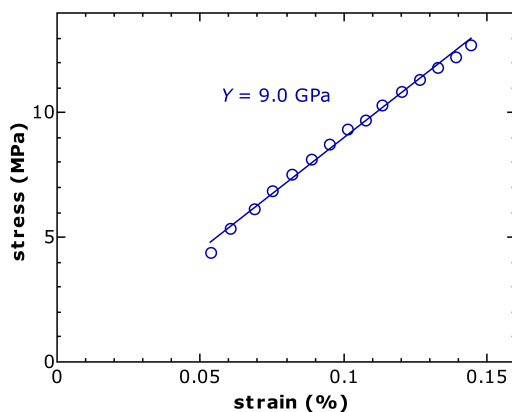


Figure S5: Representative stress-strain diagram extracted from a bulge test of a 6DT interlinked GNP membrane. The solid line depicts the slope fit yielding a biaxial modulus of $Y = 9.0$ GPa.

Pressure sweep measurements

The resistance and pressure time traces of the pressure sweeps conducted for recording the sensor's transfer function shown in figure 2 in the main document are depicted in figure S6:

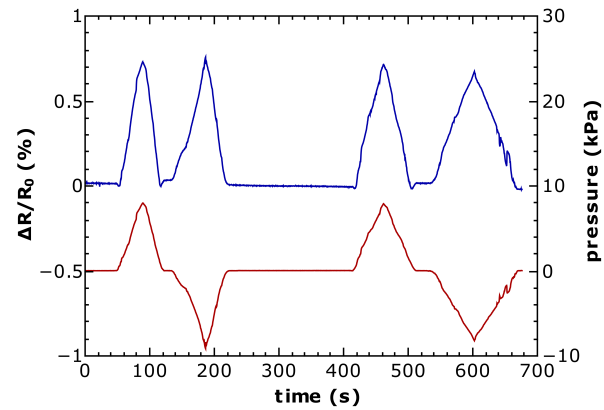


Figure S6: Resistance (*blue*) and pressure (*red*) time traces obtained by pressure sweeps for recording the sensor's transfer function.

Theoretical estimation of the sensor response

In figure 2c of the main document an estimate of the sensor response is depicted (dashed red curve). In the following, the underlying model is described.

For bulge tests on rectangular apertures, the membrane deflection at a given pressure difference can be calculated using equation 1:⁵

$$\Delta P(h) = P_{in} - P_{ex}(h) = \frac{C_1 \sigma_0 t}{a^2} h + \frac{C_2 E t}{a^4} h^3 \quad (1)$$

Here, P_{in} is the internal bulge pressure, P_{ex} is the pressure of the surrounding, h is the bulge height of the membrane's center, σ_0 is the residual stress of the membrane, t is the membrane thickness, a denotes the half width of the aperture, $E = Y(1 - \nu)$ represents the membrane material's Young's modulus and C_1 and C_2 are constants based on the bulge geometry. For bulge experiments on rectangular apertures with an aspect ratio of ≥ 4 , the constants become independent of the membrane shape and assume the following values:

$$\begin{aligned} C_1 &= 2 \\ C_2 &= \frac{4}{3(1 - \nu^2)} \end{aligned} \quad (2)$$

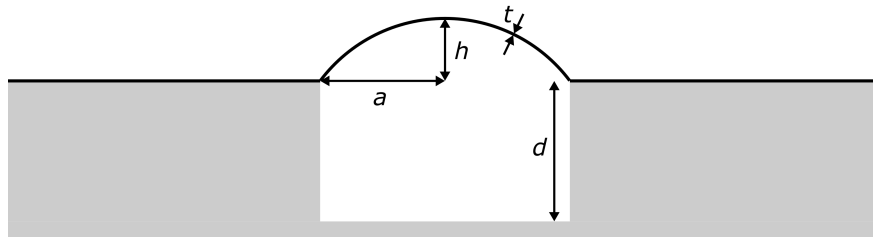


Figure S7: Schematic depicting a cross-sectional view of a membrane bulged on a rectangular cavity with annotations for the bulge height h , half aperture width a , cavity depth d and the membrane thickness t .

Here ν is the Poisson ratio of the membrane material. For all calculations we implied a cavity geometry having an aspect ratio sufficient to describe the membrane bulge section screened by the electrodes with a constant bulge height along the cavity length. This assumption applies for the device geometries used in this study.

In a bulge test, the pressure P_{in} is sourced from a large reservoir. Thus, both pressures P_{in} as well as the external pressure P_{ex} can be assumed to be constant. In our case, P_{ex} (pressure in the measurement cell) is varied in the range ± 8 kPa, resulting in a deflection of the membrane. The micrometer-range deflection of the membrane sealing the microcavity leads to changes of the cavity volume and hence to changes of the internal cavity pressure P_{in} , which can not be neglected. Thus, the internal cavity pressure P_{in} is a function of the bulge height. Equation 1 translates to:

$$P_{ex}(h) = P_{in}(h) - \frac{C_1 \sigma_0 t}{a^2} h - \frac{C_2 E t}{a^4} h^3 \quad (3)$$

$P_{in}(h)$ is expressed by the initial internal cavity pressure $P_{in,0}$ and the change in the cavity volume. The initial cavity volume (assuming a flat membrane sealing the cavity) is given by its dimensions $V_0 = ld2a$ (length l , depth d and width $2a$):

$$P_{in}(h) = P_{in,0} \frac{V_0}{V_0 + \Delta V(h)} \quad (4)$$

The volume change is given by the volume of the bulge, which is approximated as a cylindrical cap and adds or subtracts to V_0 , depending on the deflection's direction:

$$\Delta V(h) = \frac{\arctan\left(\frac{h}{a}\right) \cdot (h^2 + a^2)^2 + ah(h^2 - a^2)}{2h^2} l \quad (5)$$

By combination of equations 3, 4 and 5, an expression relating the external pressure

(pressure in the measurement cell) P_{ex} and the bulge height h can be obtained. From the bulge height h , the strain of the membrane ε (change in arc length relative to $2a$) can be approximated:

$$\varepsilon = \frac{2h^2}{3a^2} \quad (6)$$

This assumption only holds for membranes which are initially flat, i.e. having positive or zero residual stress. Implying the gauge factor G_s , which is assumed to be constant in the observed strain range⁶ and taking into account the active area of the sensor (freestanding membrane width $2a$ vs. electrode distance c) the sensor response can be approximated as follows:

$$\frac{\Delta R}{R_0}(h) = \frac{2h^2}{3a^2} G_s \frac{2a}{c} \quad (7)$$

The transfer function depicted in the main document is obtained by parametrically plotting $\frac{\Delta R}{R_0}(h)$ against $P_{ex}(h) - P_{in,0}$ in a bulge height range of $-1.2 \mu\text{m} \leq h \leq 1.2 \mu\text{m}$. In the following, the parameters assumed for calculating the estimated transfer function depicted in figure 2c (main document) are listed:

Table S1: Parameters assumed for sensor response estimation

Cavity depth	$d =$	40 μm
Cavity width	$2a =$	40 μm
Electrode distance	$c =$	80 μm
Membrane thickness	$t =$	55 nm
Biaxial modulus	$Y =$	8.9 GPa
Poission ratio	$\nu =$	0.33 ³
Initial Cavity Pressure	$P_{in,0} =$	1×10^5 Pa
Gauge factor	$G_s =$	7 ^a
Residual membrane stress	$\sigma_0 =$	6 MPa ^a

^a These parameters were obtained by matching the estimated response with the experimental data.

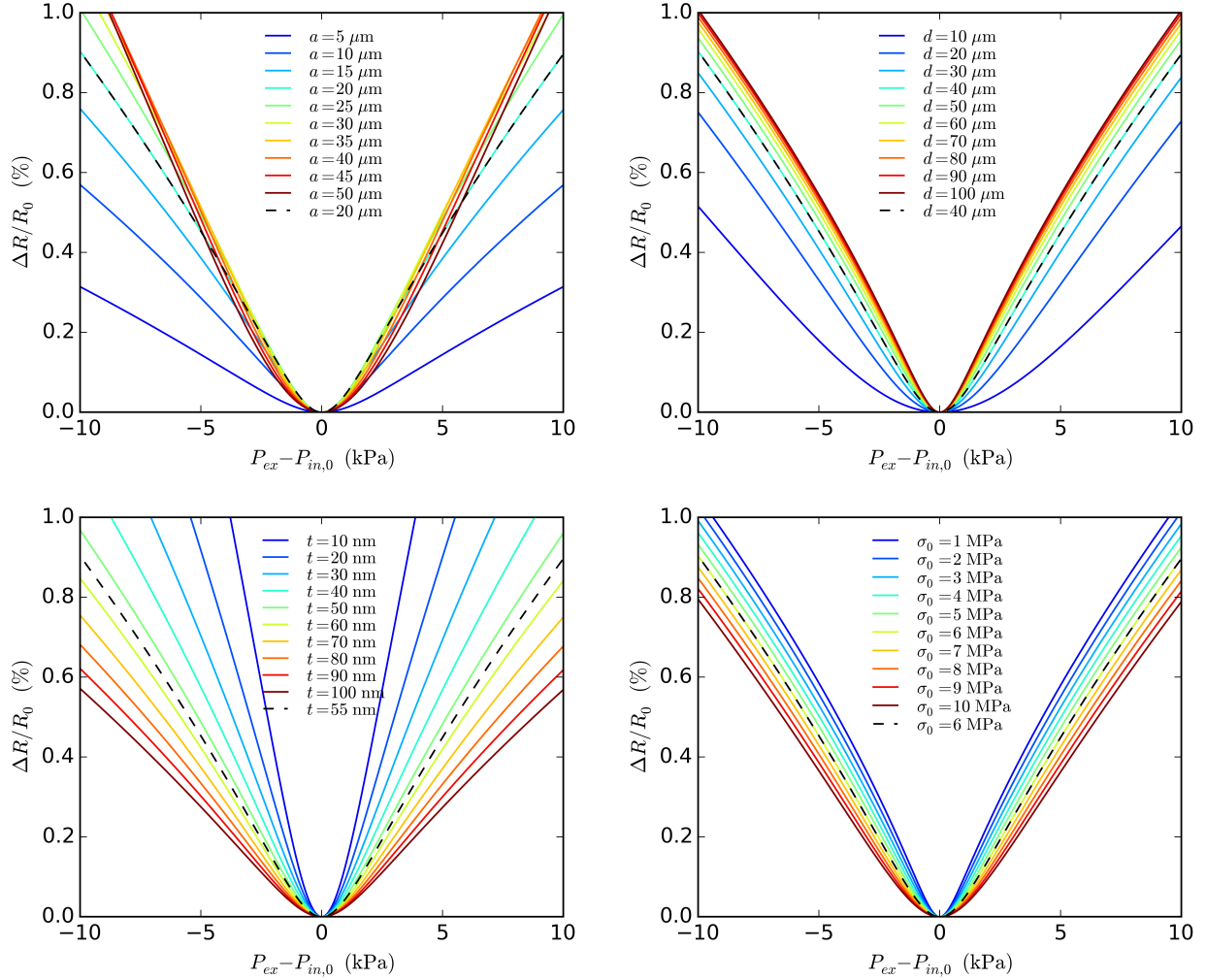


Figure S8: Predicted sensor transfer functions calculated using the parameters from table S1. The graphs show the initial transfer function (dashed black line) and curves obtained by varying the half aperture width a while scaling c proportionally to extract the influence of the bulge geometry (*top left*), varying the cavity depth d (*top right*), the membrane thickness t (*bottom left*) and the residual stress parameter σ_0 (*bottom right*).

Figure S8 depicts the estimated transfer function calculated using the parameters from table S1 as well as predicted curves under variations of different device parameters. It can be seen that the sensor response is weaker for thicker membranes or membranes having higher residual stresses after deposition, as higher pressure differences are necessary to bulge the membrane to the same extent (in terms of the change in arc length). A reduction of the aperture width $2a$ also leads to a decrease of the sensor response. Increasing the aperture width, a slight increase of sensitivity is estimated until a maximum of sensitivity could be reached. However, widening the cavity will disproportionately complicate the fabrication of larger-scale defect-free freestanding membranes. Reducing the volume of the pressure reservoir by decreasing the cavity depth d lowers the sensitivity as the pressure drop in the microcavity upon bulging is more pronounced in this case.

Pressure cell setup

Figure S9 depicts a schematic of the setup used for applying external pressures to the devices under test. It consists of a series of two needle valves, suitable to generate pressures relative to ambient from 0 to 10 kPa using a nitrogen back pressure from a gas tank or 0 to -10 kPa using a vacuum pump. The pressure, monitored by a digital pressure sensor P_2 can be adjusted and then forwarded to the pressure cell. Its pressure is monitored by another digital pressure sensor P_1 .

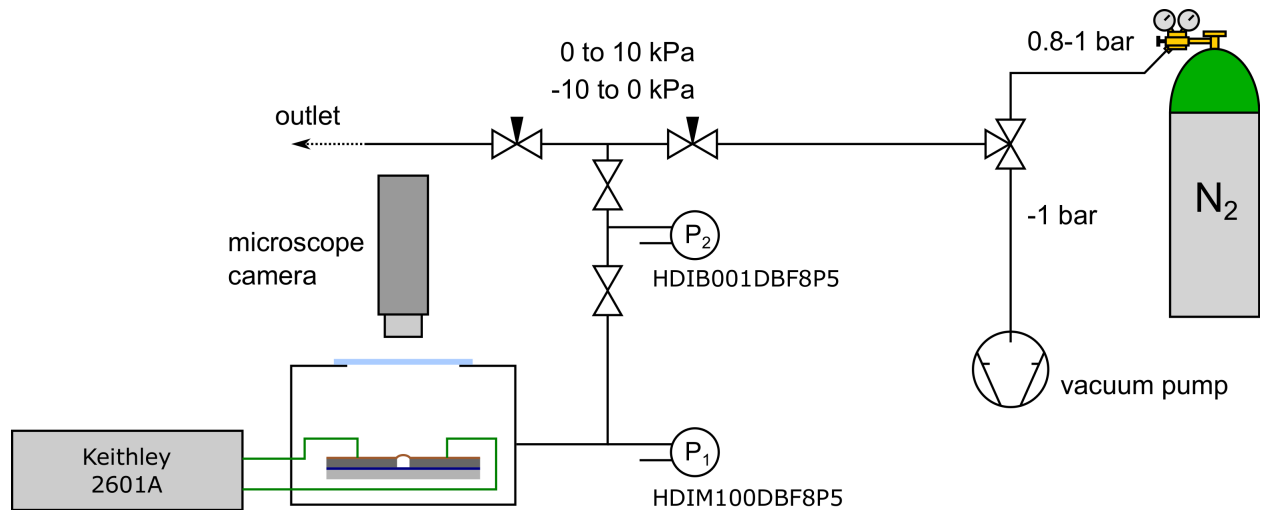


Figure S9: Setup used for characterization of the pressure sensor.

Fabrication of 3d electrode microstructures

General procedure: Optical lithography was used to fabricate 3d electrode microstructures. In a first step rectangular cavities (width ranging from $\sim 20\ \mu\text{m}$ to $\sim 80\ \mu\text{m}$ and length ranging from $\sim 500\ \mu\text{m}$ to $\sim 620\ \mu\text{m}$) were lithographically fabricated using a SU-8 50 photoresist layer on a thermally oxidized silicon wafer. Subsequently, AZ nLOF 2035 photoresist was used as a sacrificial layer in order to structure the top electrodes. In a last step either $\sim 40\ \text{nm}$ of gold were deposited by thermal evaporation or $\sim 40\ \text{nm}$ of platinum were deposited by sputtering.

Detailed description: First, a layer of SU-8 50 (MicroChem) photoresist was deposited onto a piece of thermally oxidized silicon wafer (Siegert Wafer, boron p-doped, $\langle 100 \rangle$, $675 \pm 25\ \mu\text{m}$ thickness, $300\ \text{nm} \pm 5\%$ SiO_2 thickness) by using a Spin Coater (K.L.M. SCC-200). After deposition, the photoresist was soft-baked using a hotplate at $65\ ^\circ\text{C}$ for 5 min and immediately afterward another hot plate at $95\ ^\circ\text{C}$ for 15 min. Subsequently the substrates were allowed to cool down to room temperature and were irradiated with UV light through a patterned chromium/glass mask (manufactured by Compugraphics Jena GmbH) using a long pass filter (Omega Optical PL-360P) and a Karl Suss MJB-3 mask aligner.

After exposure, the substrate was immediately post-exposure baked at $65\ ^\circ\text{C}$ for 1 min and at $95\ ^\circ\text{C}$ for 4 min. Once the sample cooled down to room temperature, the substrate was developed for 5.5 min under agitation using mr-Dev600 (micro resist technology). Following development, the substrate was rinsed with fresh mr-Dev 600 and isopropyl alcohol. After all contamination have been removed, the substrate was dried in a gentle stream of nitrogen.

In order to enhance cross-linking of the photoresist and to reduce cracks which may form during the fabrication process, the SU-8 samples were hardbaked. The hardbaking step was conducted on a hotplate, starting from $120\ ^\circ\text{C}$ up to $200\ ^\circ\text{C}$, within $\sim 10\ \text{min}$. This

temperature was held for 30 min before being cooled back to room temperature. In a second step, electrodes were deposited onto the SU-8 3d structures. To do so, one layer of AZ nLOF 2035 was spincoated at 33 rps for 60 s and soft-baked for 2 min at 110 °C. After that another layer was spincoated in the same procedure. Then a third layer was spincoated at 33 rps for 60 s and soft-baked for 4 min at 110 °C.

After the samples cooled down to room temperature, the photoresist was irradiated with UV light through a patterned negative chromium/glass photomask, yielding $\sim 300 \mu\text{m}$ wide electrodes which were placed $20 \mu\text{m}$ beside the cavity. Following exposure, the substrate was post-exposure-baked on a hotplate for 1 min at 120 °C and then cooled to ambient temperature. Dissolution of the unexposed photoresist areas was achieved by immersing the sample into AZ 726 MIF (AZ Electronic Materials) developer for 2 min. Subsequently, the substrate was rinsed briefly with fresh developer, then with ultrapure water and dried in a gentle stream of nitrogen. After the second (sacrificial) photoresist layer have been structured, $\sim 40 \text{ nm}$ of gold were deposited onto the photoresist layer by thermal evaporation (UNIVEX 350G Oerlikon Leybold Vacuum) or $\sim 40 \text{ nm}$ of Platinum were deposited onto the photoresist layer by Sputtering (GATAN Model 682 Precision Etching and Coating System (PECS)). To remove the layer of gold or platinum in the exposed areas, the substrate was immersed into TechniStrip NI555 (TECHNIC) at 80 °C for 1 hour. Due to remaining residues of gold at the edge of the SU-8 layer, the substrate was placed in an ultrasonic bath (Bandelin Sonorex RK 255 H) for a few seconds. Subsequently, the structure was rinsed in acetone, isopropanol, ultrapure water and dried in a gentle stream of nitrogen.

References

- (1) Leff, D. V.; Brandt, L.; Heath, J. R. Synthesis and Characterization of Hydrophobic, Organically-Soluble Gold Nanocrystals Functionalized with Primary Amines. *Langmuir* **1996**, *12*, 4723–4730.
- (2) Schlicke, H.; Schröder, J. H.; Trebbin, M.; Petrov, A.; Ijeh, M.; Weller, H.; Vossmeier, T. Freestanding Films of Crosslinked Gold Nanoparticles Prepared via Layer-by-Layer Spin-Coating. *Nanotechnology* **2011**, *22*, 305303.
- (3) Schlicke, H.; Leib, E. W.; Petrov, A.; Schröder, J. H.; Vossmeier, T. Elastic and Viscoelastic Properties of Cross-Linked Gold Nanoparticles Probed by AFM Bulge Tests. *J. Phys. Chem. C* **2014**, *118*, 4386–4395.
- (4) Schlicke, H.; Battista, D.; Kunze, S.; Schröter, C. J.; Eich, M.; Vossmeier, T. Freestanding Membranes of Cross-Linked Gold Nanoparticles: Novel Functional Materials for Electrostatic Actuators. *ACS Appl. Mater. Interfaces* **2015**, *7*, 15123–15128.
- (5) Schweitzer, E.; Göken, M. In Situ Bulge Testing in an Atomic Force Microscope: Microdeformation Experiments of Thin Film Membranes. *J. Mater. Res.* **2011**, *22*, 2902–2911.
- (6) Vossmeier, T.; Stolte, C.; Ijeh, M.; Kornowski, A.; Weller, H. Networked Gold-Nanoparticle Coatings on Polyethylene: Charge Transport and Strain Sensitivity. *Adv. Funct. Mater.* **2008**, *18*, 1611–1616.